1-1-2012

A Database for Estimating Organ Dose for Chest and Head CT Scans for Arbitrary Spectra and Angular Tube Current Modulation

Franco Rupcich
Marquette University

Andreu Badal

Iacovos Kyprianou

Taly Gilat Schmidt
Marquette University, tal.gilat-schmidt@marquette.edu

Published version. *Medical Physics*, Vol. 39, No. 9 (2012): 5336-5346. Permalink.

A Database for Estimating Organ Dose for Coronary Angiography and Brain Perfusion CT Scans For Arbitrary Spectra and Angular Tube Current Modulation

Franco Rupcich
Department of Biomedical Engineering, Marquette University
Milwaukee, WI
Andreu Badal
Division of Imaging and Applied Mathematics (OSEL/CDRH)
US Food and Drug Administration
Silver Spring, MD
Iacovos Kyprianou
Division of Imaging and Applied Mathematics (OSEL/CDRH)
US Food and Drug Administration
Silver Spring, MD
Taly Gilat-Schmidt
Department of Biomedical Engineering, Marquette University
Milwaukee, WI

Medical Physics, Vol. 39, No. 9 (September 2012): pg. 5336-5346. DOI.

Abstract

Purpose: The purpose of this study was to develop a database for estimating organ dose in a voxelized patient model for coronary angiography and brain perfusion CT acquisitions with any spectra and angular tube current modulation setting. The database enables organ dose estimation for existing and novel acquisition techniques without requiring Monte Carlo simulations.

Methods: The study simulated transport of monoenergetic photons between 5 and 150 keV for 1000 projections over 360° through anthropomorphic voxelized female chest and head (0° and 30° tilt) phantoms and standard head and body CTDI dosimetry cylinders. The simulations resulted in tables of normalized dose deposition for several radiosensitive organs quantifying the organ dose per emitted photon for each incident photon energy and projection angle for coronary angiography and brain perfusion acquisitions. The values in a table can be multiplied by an incident spectrum and number of photons at each projection angle and then summed across all energies and angles to estimate total organ dose. Scanner-specific organ dose may be approximated by normalizing the database-estimated organ dose by the database-estimated $CTDI_{vol}$ and multiplying by a physical $CTDI_{vol}$ measurement. Two examples are provided demonstrating how to use the tables to estimate relative organ dose. In the first, the change in breast and lung dose during coronary angiography CT scans is calculated for reduced kVp, angular tube current modulation, and partial angle scanning protocols relative to a reference protocol. In the second example, the change in dose to the eye lens is calculated for a brain perfusion CT acquisition in which the gantry is tilted 30° relative to a nontilted scan.

Results: Our database provides tables of normalized dose deposition for several radiosensitive organs irradiated during coronary angiography and brain perfusion CT scans. Validation results indicate total organ doses calculated using our database are within 1% of those calculated using Monte Carlo simulations with the same geometry and scan parameters for all organs except red bone marrow (within 6%), and within 23% of published estimates for different voxelized phantoms. Results from the example of using the database to estimate organ dose for coronary angiography CT acquisitions show 2.1%, 1.1%, and −32% change in breast dose and 2.1%, −0.74%, and 4.7% change in lung dose for reduced kVp, tube current modulated, and partial angle protocols, respectively, relative to the reference protocol. Results show −19.2% difference in dose to eye lens for a tilted scan relative to a nontilted scan. The reported relative changes in organ doses are presented without quantification of image quality and are for the sole purpose of demonstrating the use of the proposed database.

Conclusions: The proposed database and calculation method enable the

Medical Physics, Vol. 39, No. 9 (September 2012): pg. 5336-5346. DOI.

estimation of organ dose for coronary angiography and brain perfusion CT scans utilizing any spectral shape and angular tube current modulation scheme by taking advantage of the precalculated Monte Carlo simulation results. The database can be used in conjunction with image quality studies to develop optimized acquisition techniques and may be particularly beneficial for optimizing dual kVp acquisitions for which numerous kV, mA, and filtration combinations may be investigated.

Key words: CT, dose, coronary angiography, brain perfusion

I. Introduction

It has been estimated that in 2006 over 67 million CT scans were performed in the United States.[1] While these scans can be crucial in diagnosing disease, they can impart from ten to several hundred times the dose received during a typical chest x-ray or mammographic screening, depending on the protocol.[2] A retrospective cohort study assessing cancer risk from CT scans taken during childhood found that when cumulative doses reach 50 mGy, the risk of leukemia almost triples, and when cumulative doses reach 60 mGy, the risk of brain cancer almost triples, although the cumulative absolute risks are small (within 10 years of the first scan for patients under 10 years of age, one excess case of leukemia and one excess case of brain cancer per 10,000 head CT scans is estimated to occur).[5] While no similar epidemiological study has established specific levels of cancer risk associated with CT scans per se for adults, risk projections in general for radiation-attributable cancer incidence have been estimated largely on the basis of radiation epidemiology studies of atomic bomb survivors. The Biological Effects of Ionizing Radiation (BEIR) VII Phase 2 report on health risks from exposure to low levels of ionizing radiation reports that women exposed to radiation at any age suffer a higher lifetime attributable risk (LAR) of cancer incidence and mortality than men exposed at the same age.[3] The risk is higher even when breast, ovarian, and uterine cancers are excluded. At least one study has suggested that there is a non-negligible LAR of cancer associated with CT coronary angiography scans that is considerably greater for women than for men.[4] Other studies have suggested increased risk of cataract formation from exposure to low levels of ionizing radiation,[6–9] and the ICRP has recently issued a statement lowering the threshold of absorbed dose in the eye lens to 0.5 Gy.[10] Such studies, coupled with the growing public safety concern over recent incidents involving

Medical Physics, Vol. 39, No. 9 (September 2012): pg. 5336-5346. DOI.

radiation overdoses during brain perfusion scans,[11] have further motivated researchers to investigate and optimize new and existing methods of reducing dose to radiosensitive organs irradiated during these scans.

Several groups have evaluated methods of reducing dose to radiosensitive organs such as the breast, including reduced kVp and tube-current modulated scans.[12–16] In addition to developing new protocols for dose reduction, studies are also required to optimize dual-kVp protocols, which involve two kVp settings, novel filtration materials, tube current modulation, and angular kVp switching methods. Many of these studies rely on organ dose estimates obtained from experimental measurements or Monte Carlo simulations. Because each proposed scan protocol may include unique scan parameters (kVp, mAs, etc.), a separate measurement or Monte Carlo simulation is required for each dose reduction scheme, which can be both costly and time consuming. Monte Carlo simulations generally require computing resources that may not always be readily available and can take an extensive amount of time to complete depending on the scan protocol, phantom resolution, and statistical uncertainty required.

One commonly used dosimetry software tool, ImPACT's CTDosimetry Calculator,[17] enables scanner-specific organ dose estimation. However, the tool cannot estimate organ dose for scan protocols involving angular tube current modulation, partial angular scanning, or arbitrary spectra. This study developed a database for estimating organ dose for a single-rotation axial coronary angiography or brain perfusion CT scan with any spectral shape and angular tube-current/voltage modulation settings. The proposed database quantifies dose to a number of radiosensitive organs as a function of both projection angle and incident photon energy so that novel acquisition methods can be investigated. The database was created using tens of thousands of Monte Carlo simulations requiring high-performance computing resources and several weeks of running time. Users of the database are able to take advantage of the precalculated data to estimate organ dose for both existing and novel acquisition techniques without requiring Monte Carlo simulations. The database includes tables quantifying $CTDI_{vol}$ in head and body CTDI phantoms in order to provide approximate conversion factors to reflect the tube output of conventional CT scanners. Overall, the proposed database is intended

Medical Physics, Vol. 39, No. 9 (September 2012): pg. 5336-5346. DOI.

to facilitate the development of dose reduction methods and optimized single and multiple kVp acquisitions, especially for researchers without the resources required to perform Monte Carlo simulations.

Ii. Materials and Methods

II.A. Monte Carlo software

Monte Carlo simulations in this study were performed with the penImaging software package,[18–20] which relies on the previously validated PENELOPE Monte Carlo radiation transport routines.[21]

II.B. Phantoms

Five separate phantoms were used in this study: (1) anthropomorphic chest, (2) anthropomorphic head, (3) anthropomorphic head tilted 30° about the coronal plane, (4) CTDI body, and (5) CTDI head.

II.B.1. Anthropomorphic chest and head phantoms

This study used the 0.5 mm voxelized anthropomorphic female phantom, Ella, from the Virtual Family,[22] representing an average-sized 26-year-old (height: 1.63 m, weight: 58.7 kg). To relax computational memory requirements, we cropped the phantom for the head and chest simulations. For the chest simulation, the phantom was cropped to the thorax, measuring 31 cm × 22 cm in the lateral and anteroposterior directions, respectively, and 30 cm in the axial direction. For the nontilted head simulation, the phantom was cropped to the head, measuring 18 cm × 23 cm in the lateral and anteroposterior directions, respectively, and 25 cm in the axial direction. For the tilted head simulation, the cropped head phantom was tilted 30° about the coronal plane, as if the patient were to tuck their chin toward their chest. Topograms of the whole body and cropped phantoms are shown in Fig. 1. To assure that the axial lengths of the cropped phantoms were sufficient to capture most scattered radiation dose, we compared organ doses between the cropped phantoms and the full phantom for a single simulated projection. Relative to the organ doses calculated when simulating the full

Medical Physics, Vol. 39, No. 9 (September 2012): pg. 5336-5346. DOI.

phantom, the cropped phantoms capture 94% of the dose for bone and muscle, and 99% of the dose for all other organs.

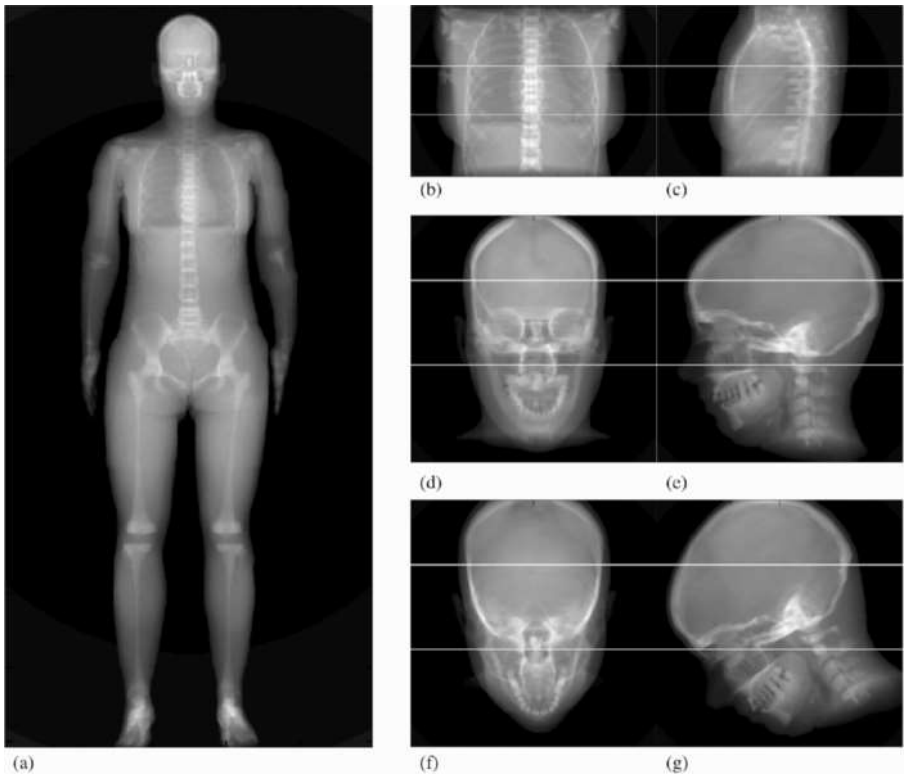

FIG. 1. (a) Topogram of the whole body (noncropped) female phantom; (b) and (c) anterioposterior and lateral topograms of the cropped chest phantom; (d) and (e) nontilted head phantom; and (f) and (g) the tilted head phantom. The scan field of view for each of the cropped phantoms is represented by the space between the white horizontal lines and corresponds to a coronary angiography scan for (b) and (c) and a brain perfusion scan for (d)–(g).

The breast was modeled as two separate parts: an internal glandular mass and an external 1-cm-thick surrounding layer of adipose. Thus, voxels representing the internal glandular mass were modeled as 100% glandular tissue, while the surrounding layers of voxels were modeled as 100% adipose. As such, "dose to breast" in the context of this study refers to dose to the 100% glandular material. Voxels representing the following organs/tissues were modeled according to their respective atomic compositions and densities as given by ICRP publication 110:[23] fat (adipose), glandular tissue, adrenals, blood, cartilage, esophagus, eye lens, stomach, heart, kidney, liver, muscle, pancreas, skin, spleen, teeth, thyroid, and

Medical Physics, Vol. 39, No. 9 (September 2012): pg. 5336-5346. DOI.

soft tissue. Voxels representing the following organs/tissues were modeled according to their respective atomic compositions and densities as given by Woodard and White:[24] lung (blood filled, 50% inflated, 50% deflated, density: 0.655 g/cm^3), cerebrospinal fluid, connective tissue. The brain was divided into three organs with slightly different atomic compositions and densities: "brain (gray matter)" including gray matter, the hippocampus and the thalamus were modeled as gray matter according to the composition given by Woodard and White;[24] "brain (white matter)" including white matter, the commissura anterior, and the commissura posterior were modeled as white matter according to the composition given by Woodard and White;[24] and "brain (mean gray/white matter)" including the cerebellum, medulla, midbrain, and pons were modeled as a 50/50 mixture of gray and white matter as defined in ICRP publication 110.[23] The diaphragm, larynx, and tongue were modeled as muscle. All skeletal voxels were modeled as homogenous bone (density: 1.4 g/cm^3) as given by Cristy and Eckerman.[25] This study quantified dose only in the organs listed in Table I. Most of these organs were fully included in the cropped phantoms except those listed in Table II, which lists the ratio of the organ mass in the cropped phantoms to the organ mass in the full phantom.

TABLE I. Dose deposition tables generated for each of the five phantoms.

Phantom	Dose tables generated
Chest	Lung
	Breast
	Esophagus
	Heart
	Bone
	Red marrow
	Skin
	Muscle
Head/Head (30 deg tilt)	Brain (gray matter)
	Brain (white matter)
	Brain (mean gray/white matter)
	Eye lens
	Bone
	Red marrow
	Skin
	Muscle
CTDI head/body	$CTDI_{vol}$

Medical Physics, Vol. 39, No. 9 (September 2012): pg. 5336-5346. DOI.

TABLE II. Fractional organ masses (ratio of organ mass in cropped phantom to full phantom). Those organs not listed in the table have a fractional mass of 1.0 (i.e., they are completely included in the cropped phantoms).

Phantom	Organ	Fractional mass
Chest	Esophagus	0.92
	Bone	0.18
	Red marrow	0.16
	Skin	0.17
	Muscle	0.18
Head/Head (30 deg tilt)	Bone	0.19
	Red marrow	0.09
	Skin	0.09
	Muscle	0.04

II.B.2. CTDI body and head phantoms

A 32-cm-diameter virtual CTDI body phantom[26] was created using simple cylindrical and planar mathematical quadrics. The five holes in which the ion chambers are placed were 100 mm long and 12.4 mm in diameter and located at the phantom center and at the 12 o'clock, 3 o'clock, 6 o'clock, and 9 o'clock positions, 1 cm interior from the surface of the phantom. The phantom was made of PMMA material (density: 1.19 g/cm^3). Each of the five ion chamber holes was also modeled as PMMA material (i.e., as if PMMA filled the holes). Dose-to-PMMA was converted to dose-to-air in order to calculate CTDIvol, which is explained in Sec. II.E.2. A virtual CTDI head phantom[26] measuring 16 cm in diameter was similarly created. Both CTDI phantoms were 15 cm in height.

II.C. Simulation geometry

The source-to-detector distance for each simulation was 100 cm, with a source-to-isocenter distance of 50 cm. We modeled a single-rotation stationary cone-beam system with no table translation and a beam width at isocenter of 8 cm, which was chosen to represent the volume scanning capabilities of 320 detector row CT scanners

Medical Physics, Vol. 39, No. 9 (September 2012): pg. 5336-5346. DOI.

during brain perfusion and coronary angiography scans.[27,28] We modeled a point source with a fan angle of 53.13°, which was wide enough to cover the entire width of each phantom.

II.D. Energy deposition simulations

The transport of monoenergetic photons through each of the five phantoms was simulated between 5 and 150 keV in 1 keV increments for 1000 projections in 0.36° increments. Monoenergetic simulations were performed for two reasons: (1) so that results may be used to investigate the effects of specific incident photon energy levels on organ dose, and (2) so that organ dose may be calculated for any polyenergetic spectral shape, as will be explained in detail in Sec. II F. For each photon energy at each projection angle, 10^7 photons emitted from the source within the collimated beam (henceforth referred to simply as "emitted photons") were tracked through the anthropomorphic and CTDI phantoms, and the energy deposited in each organ or material of interest for each phantom was tallied. A bowtie filter corresponding to that used for head protocols of a Toshiba Aquilion 64 scanner,[29] and a bowtie filter corresponding to that used for body protocols of a Siemens AS+ scanner[30] were modeled by calculating the fan-angle dependent transmission spectra at each incident photon energy for the same materials and thicknesses representative of the physical bowtie attenuation characteristics described in Abboud *et al.*[29] and McKenney *et al*.[30] These head and body bowtie spectra were then used for the radiation-transport simulations respective of the head and chest phantoms of this study (Sec. II B).

II.E. Organ dose tables

A table of normalized dose deposition, $Q_O(\theta, E)$, quantifying the dose to organ, O, per emitted photon (mGy/emitted photon) for each incident photon energy, E, and projection angle, θ, was generated for the organs of the phantoms listed in Table I. Figure 1 shows the scan field of view (FOV) for the simulations of the anthropomorphic chest and head phantoms. Sections II.E.1–II.E.3 describe how the tables were generated.

Medical Physics, Vol. 39, No. 9 (September 2012): pg. 5336-5346. DOI.

II.E.1. Nonskeletal dosimetry

For each organ of interest except the bone and red bone marrow (explained separately in Sec. II.E.2), the energy deposited (reported in eV per emitted photon), was converted to dose by converting eV to Joules and dividing by the mass of the organ in the respective cropped phantom. These calculations resulted in tables of normalized dose deposition, $Q_O(\theta, E)$, quantifying the dose to organ, O, per emitted photon (mGy/emitted photon) for each incident photon energy, E, and projection angle, θ.

II.E.2. Skeletal dosimetry

Due to the difficulty in accurately modeling the anatomical microstructure of trabecular spongiosa, doses to the radiosensitive red marrow cells and bone surface cells contained within the skeletal tissue are often approximated using one of several widely accepted techniques.[31] We approximated dose to bone as dose to the homogenous bone material described in Sec. II.B.1, using the same method of converting from energy deposited to dose as described in Sec. II.E.1, and using the mass of bone in the respective cropped phantoms. These calculations resulted in a table of normalized dose deposition for homogenous bone, $Q_{HB}(\theta, E)$.

We used Eq. (1), originally proposed by Rosenstein[32] and employed by Turner *et al.*,[33] to estimate the dose to red bone marrow from the dose to homogenous bone:

$$D_{RBM} = D_{HB} \cdot \frac{(\mu_{en}/\rho)_{RBM}}{(\mu_{en}/\rho)_{HB}}, \quad (1)$$

where D_{RBM} and D_{HB} are the doses to red bone marrow and homogenous bone, respectively, and $(\mu_{en}/\rho)_{RBM}$ and $(\mu_{en}/\rho)_{HB}$ are the mass energy absorption coefficients of red bone marrow and homogenous bone. We created the table of normalized dose deposition for red bone marrow by using Eq. (1) and the table of normalized dose deposition for homogenous bone. To calculate the table of normalized dose deposition for homogenous bone for each phantom, we divided the energy deposited by the mass of the homogenous bone in the

Medical Physics, Vol. 39, No. 9 (September 2012): pg. 5336-5346. DOI.

cropped phantoms. The mass energy absorption coefficients of both materials were calculated using Eq. (2):

$$(\mu_{\text{en}}/\rho)_{\text{material}} = \sum_i w_i \cdot (\mu_{\text{en}}/\rho)_i, \quad (2)$$

where w_i is the percent composition by mass and $(\mu_{en}/\rho)i$ is the mass energy absorption coefficient of the ith element comprising the material. Elemental percent compositions for red bone marrow were taken from Woodard and White,[24] while those for homogenous bone were taken from Cristy and Eckerman.[25] Elemental mass energy absorption coefficients were obtained from tables published by Hubbell and Seltzer.[34]

II.E.3. $CTDI_{vol}$ tables

We also created tables quantifying the $CTDI_{vol}$ in mGy per emitted photon for both the head and body CTDI phantoms. First, the $CTDI_{100}$ at each incident photon energy for both the center and peripheral chambers of the CTDI phantoms were obtained using Eq. (3):

$$\text{CTDI}_{x,100} = \frac{E_x \cdot e \cdot L}{m \cdot N \cdot T} \cdot 1000 \cdot \frac{(\mu_{\text{en}}/\rho)_{\text{AIR}}}{(\mu_{\text{en}}/\rho)_{\text{PMMA}}}, \quad (3)$$

where $CTDI_{x,\ 100}$ is the $CTDI_{100}$ at the center ($CTDI_{c,\ 100}$) or periphery ($CTDI_{p,\ 100}$) chamber of the CTDI phantom, E_x is the total energy deposited in the center or peripheral chamber (eV/emitted photon), *e* is the electron charge constant (conversion factor from eV to Joules), *L* is the active length of the chamber (10 cm), *N* is the number of slices, *T* is the tomographic section thickness [$N \cdot T$ is the nominal beam width (8 cm)], *m* is the mass of PMMA in the chamber, the factor of 1000 is used to convert from Gy to mGy, and $(\mu_{en}/\rho)_{AIR}$ and $(\mu_{en}/\rho)_{PMMA}$ are the mass energy absorption coefficients for air and PMMA, respectively. Multiplying by the ratio of the mass energy absorption coefficients converts dose-to-PMMA to dose-to-air. The method of modeling the ion chambers as PMMA and converting to dose-to-air has been previously validated.[35] Mass energy absorption coefficient values for air and PMMA were obtained from Hubbell and Seltzer.[34]

Medical Physics, Vol. 39, No. 9 (September 2012): pg. 5336-5346. DOI.

$CTDI_w$ was then calculated using Eq. (4):[36]

$$CTDI_w = 1/3 \cdot CTDI_{c,100} + 2/3 \cdot CTDI_{p,100}. \quad (4)$$

Because $CTDI_{vol}$ is equal to $CTDI_w$ divided by the pitch, and since we used a pitch of one, our $CTDI_{vol}$ is equivalent to $CTDI_w$.

II.F. Using the database to estimate dose

The total dose to an organ, D_O, for a scan can be calculated using Eq. (5):

$$D_O = \sum_{\theta} N_0(\theta) \sum_{E} \Phi(\theta, E) Q_O(\theta, E), \quad (5)$$

where $N_0(\theta)$ is the number of emitted photons at projection angle, θ; $\Phi(\theta, E)$ is the fraction of photons incident at projection angle, θ, with energy, E (i.e., the spectral distribution at projection angle, θ); and $Q_O(\theta, E)$ is the table of normalized dose deposition (i.e., dose to organ, O, per emitted photon at angle, θ, and energy, E, as described in Sec. II.E.1). As seen in Eq. (5), the total organ dose is a linear combination of the values in the table of normalized dose deposition for that organ with the weights dependent on the spectrum and number of emitted photons at each projection angle.

The table of normalized dose deposition, $Q_O(\theta, E)$, for each organ is the output of the presented Monte Carlo simulations for the specific CT geometry we have described, while $N_0(\theta)$ and $\Phi(\theta, E)$ are user-modifiable parameters. Together, $N_0(\theta)$ and $\Phi(\theta, E)$ represent an input x-ray spectrum. Modifying these two parameters allows for calculating total organ dose for various acquisition methods, filtration schemes, and scan parameters. For example, tube voltage settings and spectra filtration can be changed by properly modifying $\Phi(\theta, E)$. While our method does not allow a user to directly specify an mAs value when calculating organ dose, a relative change in mAs by a certain factor between protocols is represented by the same relative change in $N_0(\theta)$ in Eq. (5), since the number of incident photons is proportional to the tube-current time-product. In this manner, $N_0(\theta)$ can be modified across rotation angle, θ, to model angular tube

Medical Physics, Vol. 39, No. 9 (September 2012): pg. 5336-5346. DOI.

current modulation. As described in Sec. II H, the database includes information about the phantoms' attenuation as a function of angle and energy to facilitate calculation of tube current modulation settings, as will be performed in Sec. II I. In addition, setting $N_0(\theta)$ to zero at desired angles represents partial-angle scanning. Angularly interlaced dual-kVp protocols can be modeled by changing $N_0(\theta)$ and $\Phi(\theta, E)$ at alternating angles.

While Eq. (5) gives an organ dose in units of mGy, this estimate depends on the selected $N_0(\theta)$ and is not indicative of organ dose from a specific scanner. Thus, Eq. (5) can be used to compare the change in organ doses between protocols, which depends on the change in $N_0(\theta)$ across protocols rather than the specific value of $N_0(\theta)$. Sections II I and II J demonstrate examples of using the database for studying changes in dose between protocols.

If the mAs-to-photon-fluence conversion factor for a specific scanner is known or measured, a realistic $N_0(\theta)$ could be determined and used with the database to obtain a dose estimate that reflects typical tube output. For example, the IPEM Report 78 software provides an estimate of these conversion factors.[37] Another approach for obtaining dose estimates for a specific scanner's output is to calculate a scaling factor using $\mathrm{CTDI_{vol}}$ normalization, as described in Eq. (6):

$$D_{\text{scanner}} = D_{\text{database}} \cdot \frac{\mathrm{CTDI_{vol,scanner}}}{\mathrm{CTDI_{vol,database}}}, \tag{6}$$

where D_{database} and $\mathrm{CTDI_{vol,\,database}}$ are the organ dose and $\mathrm{CTDI_{vol}}$, respectively, calculated using the dose tables. $\mathrm{CTDI_{vol,\,scanner}}$ is the $\mathrm{CTDI_{vol}}$ measured on the scanner of interest using the same spectrum, $\Phi(\theta, E)$, as that used from the dose table estimations. This scaling factor adjusts for differences in scanner output and has been previously validated by Turner *et al*. for fully irradiated organs in abdominal scans with constant tube current.[33,38] Our database, however, presents organ dose data for coronary angiography and brain perfusion scans and for partially irradiated organs, therefore the conversion presented in Eq. (6) is expected to provide an approximate

Medical Physics, Vol. 39, No. 9 (September 2012): pg. 5336-5346. DOI.

estimate of scanner-specific organ dose. A preliminary validation of the organ dose estimates normalized by $CTDI_{vol}$ is presented in Sec. II G.

As explained in Secs. II.E.1 and II.E.2, we estimated the organ dose in the dose deposition tables by dividing energy deposited in an organ by the mass of the organ in the cropped phantom. For those organs that are not completely included in the cropped phantoms (see Table II), this method of evaluation can lead to an overestimate of the *whole*-organ dose. If whole-organ dose is desired, then the organ dose estimate obtained using Eq. (5) should be adjusted using the fractional mass values of Table II.

II.G. Validation

PENELOPE's Monte Carlo routines have been previously validated.[21] To validate that the linear combination of database values [Eq. (5)] does not introduce additional biases, we compared organ doses estimated by the database to those estimated by Monte Carlo simulations of the cropped head and chest phantoms, each consisting of 1000 views, 10^9 emitted photons per view, and a 120 kVp polyenergetic spectrum generated using the IPEM Report 78 software[37] (tungsten target, 12° anode angle, 0% voltage ripple, and 6 mm aluminum filtration). The scan geometry was identical to that used to generate the tables of normalized dose deposition, $Q_O(\theta, E)$, described in Sec. II C. The total dose to each organ output from these simulations was compared to that calculated using Eq. (5) assuming the 120 kVp spectrum and 10^9 emitted photons per view.

A study was also performed to validate the organ dose estimates normalized by the $CTDI_{vol}$ estimates, which can be used to adjust the database dose estimates to reflect realistic scanner output [Eq. (6)]. In this study, the breast and lung doses per $CTDI_{vol}$ estimated by the database were compared to those reported by Turner *et al*. from Monte Carlo simulations of a different voxelized phantom. The Turner study found that organ dose per $CTDI_{vol}$ is generally scanner independent.[33] However, the entire breast and lung were irradiated in the Turner study, while only a portion of the breast and lung were irradiated in our system geometry. Therefore, the organ dose per $CTDI_{vol}$ estimated from the database was scaled by the

Medical Physics, Vol. 39, No. 9 (September 2012): pg. 5336-5346. DOI.

fraction of irradiated organ volume (57.7% for breast, 49.7% for lung) prior to comparison to Turner's values.

II.H. Obtaining patient attenuation data

Analytical ray-tracing was performed to determine the attenuation at each incident photon energy and projection angle for the anthropomorphic head, tilted head, and chest phantoms. The attenuation was defined as the inverse of the transmission (i.e., $A = e^{\mu \cdot L}$) averaged over the central 100 pixels (2.5 cm) of the detector. The attenuation data can be used in modeling attenuation-based tube-current modulation schemes, as will be demonstrated in Sec. II I.

II.I. Example 1: Using the dose database to investigate change in dose to breast

In this section, we demonstrate how to use the dose database to calculate the change in dose to the breast for three protocols commonly used to reduce breast dose—reduced kVp, partial scanning, and angular tube current modulation. Because acquisition techniques designed to reduce breast dose may increase lung dose, we also estimate the subsequent change in dose to the lung for each protocol. Changes in organ dose are reported relative to a 120 kVp reference protocol.

II.I.1. Reference 120 kVp protocol

The total dose to the breast for the reference protocol was calculated using Eq. (5) and $Q_{\text{breast}}(\theta, E)$. $\Phi(\theta, E)$ was set equal to a normalized 120 kVp spectrum for all θ. Since we are interested only in change in dose, the absolute number of emitted photons used in Eq. (5) is irrelevant. Therefore, we set the number of emitted photons per view, $N_0(\theta)$, equal to one for all θ (Fig. 2). Similarly, we used Eq. (5) with $Q_{\text{lung}}(\theta, E)$ to calculate total dose to the lung.

Medical Physics, Vol. 39, No. 9 (September 2012): pg. 5336-5346. DOI.

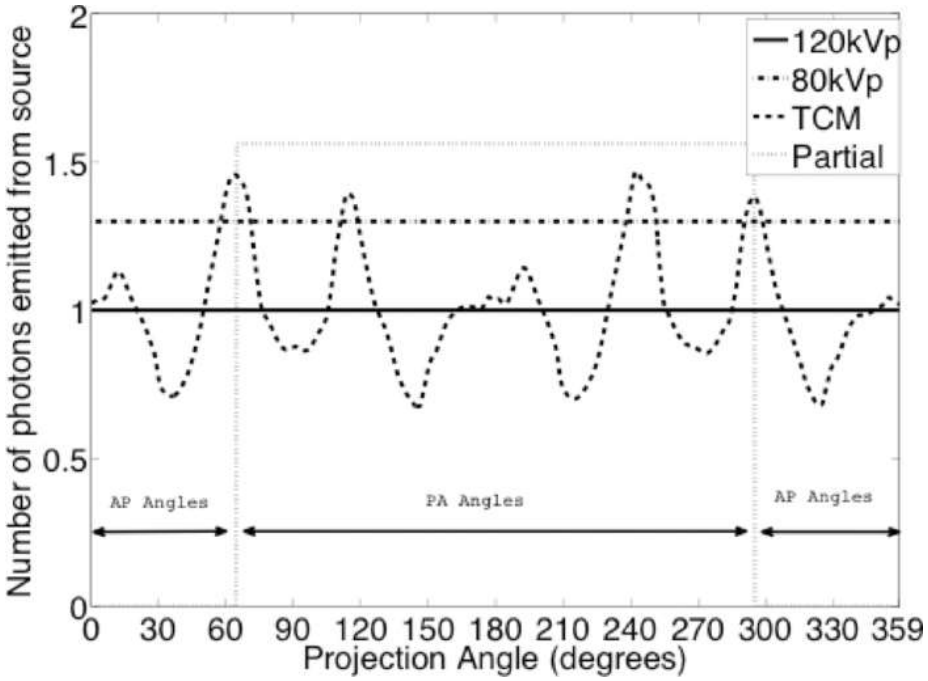

FIG. 2. $N_0(\theta)$ for the protocols listed in Sec. II I. The area under the curve [i.e., $N_0(\theta)$ summed across all angles] is equal for the 120 kVp, tube-current modulation, and partial scan protocols, while the 80 kVp protocol has 1.3 times the number of emitted photons from the source.

II.I.2. Reduced kVp protocol

The total dose to the breast for the 80 kVp protocol was calculated using Eq. (5) and $Q_{\text{breast}}(\theta, E)$. $\Phi(\theta, E)$ was set equal to a normalized 80 kVp spectrum for all θ. We had previously determined that to obtain a noise variance similar to that of the 120 kVp protocol, the number of emitted photons at each angle of the 80 kVp protocol should be increased by a factor of 1.3 relative to the 120 kVp protocol.[39] Thus we set $N_0(\theta)$ equal to 1.3 for all θ (Fig. 2). Similarly, we used Eq. (5) with $Q_{\text{lung}}(\theta, E)$ to calculate total dose to the lung.

II.I.3. Tube current modulation protocol

The total dose to the breast for this protocol was calculated using Eq. (5) and $Q_{\text{breast}}(\theta, E)$. $\Phi(\theta, E)$ was set equal to a normalized 120 kVp spectrum for all θ. Using the patient attenuation data, an optimal attenuation-based tube-current modulation scheme was modeled in which the number of emitted photons at each angle, $N_0(\theta)$, was proportional to the square root of the attenuation at that angle,

Medical Physics, Vol. 39, No. 9 (September 2012): pg. 5336-5346. DOI.

$\sqrt{A(\theta)}$, [40] while the total number of emitted photons for the scan remained the same as in the reference protocol (Fig. 2). Similarly, we used Eq. (5) with $Q_{lung}(\theta, E)$ to calculate total dose to the lung.

II.I.4. Partial angle protocol

The total dose to the breast for this protocol was calculated using Eq. (5) and $Q_{breast}(\theta, E)$. $\Phi(\theta, E)$ was set equal to a normalized 120 kVp spectrum for all θ. We set $N_0(\theta)$ equal to zero during the 360 projections (130°) centered about AP and to 1.56 during the remaining 640 projections (230°). These factors were chosen to represent the x-ray tube giving no output during the AP views and increased output during the PA views such that the total number of emitted photons for the entire 360° scan remained the same as in the reference protocol (Fig. 2). Similarly, we used Eq. (5) with $Q_{lung}(\theta, E)$ to calculate total dose to the lung.

II.J. Example 2: Using the dose database to investigate change in dose to eye lens

In this section, we demonstrate how to use the dose database to calculate the change in dose to the eye lens for a tilted head scan relative to a nontilted scan.

II.J.1. Reference (non-tilted) protocol

The total dose for the reference protocol was calculated using Eq. (5) and $Q_{eye}(\theta, E)$ for nontilted head phantom. We set $\Phi(\theta, E)$ equal to a normalized 80 kVp spectrum for all θ, and we set the number of emitted photons per view, $N_0(\theta)$, equal to one for all θ.

II.J.2. Tilted protocol

The same method used for the nontilted protocol was used to calculate the total dose except that in Eq. (5) we used the table of normalized dose deposition, $Q_{eye}(\theta, E)$, for the tilted head phantom.

Medical Physics, Vol. 39, No. 9 (September 2012): pg. 5336-5346. DOI.

III. RESULTS

III.A. Dose tables

Our simulations resulted in a table of normalized dose deposition, $Q_O(\theta, E)$, for each of the organs (or $CTDI_{vol}$) of the phantoms listed in Table I, quantifying the dose per emitted photon (mGy/emitted photon) for each incident photon energy, E, and projection angle, θ. Head[29] and body[30] bowtie filters were modeled for the simulations. Examples of tables of normalized dose deposition for the breast, lung, eye lens, and brain (gray matter) are shown in Fig. 3. Viewing the tables graphically may provide insight for designing new protocols, since the projection angles and energies that deposit the most dose can be visualized. The uncertainty of the normalized dose deposition values varied across photon energy, projection angle, and organ. For example, the uncertainty in breast dose for the PA projection was 2.92% at 20 keV and 0.16% at 120 keV. When calculating the organ dose using Eq. (5), the individual statistical uncertainties at each incident photon energy and projection angle propagate such that the total statistical uncertainty for a calculated total organ dose or $CTDI_{vol}$ for a given spectrum and number of emitted photons is on the order of 0.0005%.

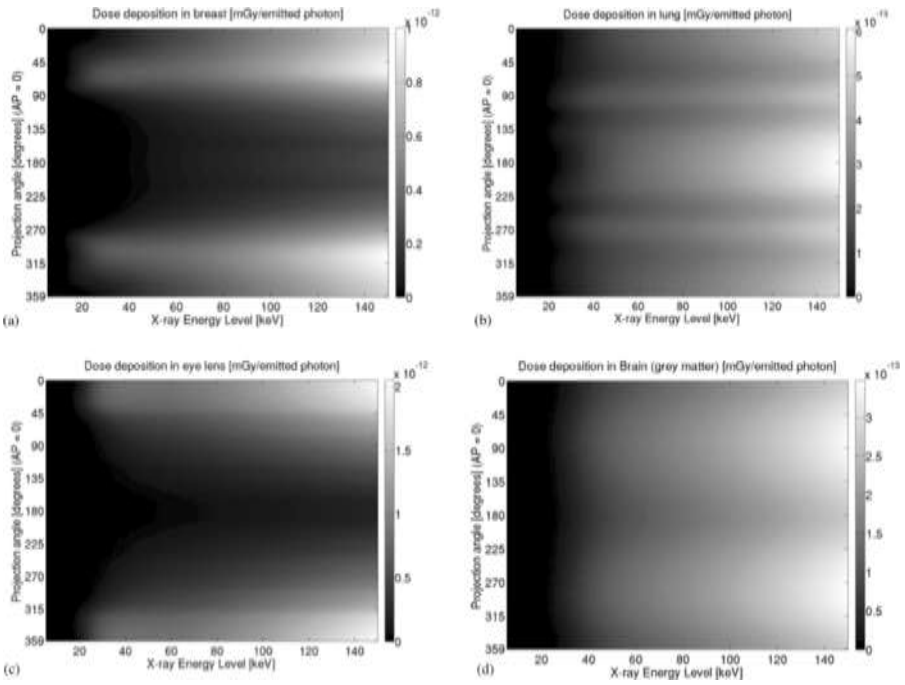

Medical Physics, Vol. 39, No. 9 (September 2012): pg. 5336-5346. DOI.

FIG. 3. Table of normalized dose deposition $Q_O(\theta, E)$ for (a) breast, (b) lung, (c) eye lens, and (d) brain (gray matter), quantifying organ dose per emitted photon (mGy/emitted photon) at each incident photon energy, E and projection angle, θ. Note that 0° and 180° correspond to AP and PA projections, respectively, and 90° and 270° correspond to left lateral and right lateral incidence, respectively.

The tables of normalized dose deposition are saved as ASCII formatted files[51] and as supplementary material.[52] In addition, the patient attenuation data for the head, tilted head, and chest phantoms are also made available for use in designing attenuation-based tube current modulation schemes.

III.B. Validation

The percent differences between total organ doses obtained from the 120 kVp polyenergetic Monte Carlo simulations and those calculated using Eq. (5) varied between −0.91% and 0.15% for all organs except the red bone marrow, which yielded a percent difference of 6.1% for coronary angiography simulation and 4.3% for the brain perfusion simulation. These results demonstrate that the database yields dose estimates comparable to those calculated using conventional Monte Carlo simulations. The larger percent differences in the red bone marrow estimates may be due to the errors involved in estimating the mass energy absorption coefficient for an energy spectrum (as is done in the case of the Monte Carlo simulation) as opposed to using the monoenergetic coefficient values (as is done when using the dose tables). The smaller percent differences for the other organs are expected due to the statistical variation inherent in results obtained via Monte Carlo simulations. The lung and breast organ doses per $CTDI_{vol}$ estimated from the database were 1.24 and 1.59, respectively (after scaling by the fraction of irradiated organ mass), compared to 1.59 and 1.77 as estimated by Turner *et al*.[33] The differences in dose per $CTDI_{vol}$ (−22% for breast and −10% for lung) are reasonable considering the anatomical differences between the phantoms used in the two studies.

III.C. Example of estimating change in dose to breast

There was a 2.1%, 1.1%, and −32% difference in dose to the breast and a 2.1%, 0.6%, and 4.7% difference in dose to the lung for the reduced kVp, tube current modulated, and partial angle scan

Medical Physics, Vol. 39, No. 9 (September 2012): pg. 5336-5346. DOI.

protocols, respectively, relative to the 120 kVp reference protocol, where a negative percentage indicates a decrease in dose (Table III).

TABLE III. The percent change in breast and lung dose for reduced kVp, tube current modulation (TCM), and partial angular scanning (partial) protocols relative to the 120 kVp reference scan. A negative percentage indicates a decrease in dose.

Scan type	Spectrum (kVp)	$N_0(\theta)$	Change in breast dose (%)	Change in lung dose (%)
Reference	120	1.00	...	...
Reduced kVp	80	1.30	2.1	2.1
TCM	120	$\propto \sqrt{A(\theta)}$	1.1	0.6
Partial	120	0.0 (130° AP) 1.56 (230° PA)	−32	4.7

III.D. Example of estimating change in dose to eye lens

There was a −19.2% difference in dose to the eye lens for tilted head scan relative to the nontilted reference protocol, where the negative percentage indicates a decrease in dose.

IV. Discussion

The presented database allows investigation of numerous dose reduction techniques with various scan parameters and protocols (e.g., x-ray spectrum, filtration, and tube-current modulation) for a specific scan geometry and voxelized phantom model without Monte Carlo simulations. Compared to available organ dose estimators,[17] our database can model novel coronary angiography and brain perfusion acquisition techniques for the scan geometry presented, thus facilitating the development and optimization of new acquisition protocols. For example, a variety of dual-kVp techniques can be modeled by changing $N_0(\theta)$ and $\Phi(\theta, E)$. The database may enable researchers with limited access to high-performance computing resources to develop novel acquisition methods. The presented

Medical Physics, Vol. 39, No. 9 (September 2012): pg. 5336-5346. DOI.

method of calculating tables of normalized dose deposition could also be applied to other CT applications. For example, several studies evaluated the impact of spectral shape on dose and image quality in breast CT.[41,42] Future work could develop dose deposition databases for phantoms and geometries specific to breast CT to enable efficient optimization of acquisition techniques.

The estimated organ dose results presented in this paper reflect changes in dose without quantifying image quality. The purpose of our examples is not to make claims with respect to dose reduction for any of the studied protocols, but to illustrate how our method can be used to estimate changes in organ dose between protocols. To determine the optimal protocol from our examples, the reported changes in dose would need to be evaluated alongside a corresponding image quality study.

IV.A. Limitations and future work

Because the data we have collected for each phantom are specific to the simulated geometries, dose estimates for helical trajectories, longitudinal tube-current modulation schemes, and FOVs other than those shown in Fig. 1 cannot be obtained directly with our database. One strength of other dose databases, including those used by ImPACT's CTDosimetry Calculator,[43,44] is that organ dose coefficients are given for each of several 5 or 10 mm thick cross-sectional slabs that together constitute a large portion of the phantom (e.g., thigh to head). With the data organized in this fashion, one can obtain the total organ dose for a particular FOV by summing all of the organ coefficients for the slabs included in that FOV. The database presented in this paper enables organ dose estimation for coronary angiography and brain perfusion scans, in particular, as these applications are of recent concern with regard to dose.[3,4,6,7,11] Future studies will aim to extend our database to include tables of normalized dose deposition for a number of thin cross-sectional slabs that together comprise the entire length of the phantom, in which case it would be possible to estimate total organ dose to all organs of the body for arbitrary FOVs and trajectory types as well as longitudinal tube-current modulation schemes.

Medical Physics, Vol. 39, No. 9 (September 2012): pg. 5336-5346. DOI.

Several studies have shown that absorbed organ dose tends to increase with decreasing patient size.[13,38,45,46] Our database presents organ dose deposition tables for one average-sized female phantom. Thus, results for relative dose reduction between protocols obtained using our database are limited to a patient of similar size. Future studies could expand the database to include smaller and larger patients, as well as pediatric and adult male phantoms, so that the effects of patient size, age, and gender on organ dose reduction for novel protocols may be investigated. Alternatively, coefficients for scaling organ dose estimates based on patient size have been investigated.[38] These scaling factors could be combined with a full-phantom database to enable more patient-size specific dose estimates from a single-phantom database.

The $CTDI_{vol}$ normalization and multiplication method proposed in Sec. II F provides an approximate conversion to scanner-specific dose estimates. At present, however, the method has not been fully validated for partially irradiated organs or a wide range of exam protocols.[33,38] This does not limit the databases ability to quantify relative organ dose differences between protocols.

Despite these limitations, the proposed database and method of estimating organ dose [Eq. (5)] can be used in conjunction with image quality studies to determine which dose reduction protocols provide the best ratio of image quality to dose. Since the database provides quantification and visualization of dose deposition across energy and projection angle, it may aid in determining optimal spectra and tube current modulation parameters. The database may be useful in understanding the dose implications of novel spectral, partial scanning, and few-view techniques, and may be particularly beneficial for developing dual kVp techniques,[47–50] for which the kV, filtration, and mA must be optimized for both the low and high energy acquisitions with respect to image quality and dose. This optimization may require numerous combinations of scan parameters, which can be easily modeled with the proposed database by modifying the spectra, $\Phi(\theta, E)$, and number of emitted photons, $N_0(\theta)$, in Eq. (5).

Medical Physics, Vol. 39, No. 9 (September 2012): pg. 5336-5346. DOI.

V. Conclusion

The proposed database and calculation method enable the estimation of organ dose for coronary angiography and brain perfusion CT scans utilizing any spectral shape and angular tube current modulation scheme without requiring Monte Carlo simulations. Overall, the proposed database facilitates development of novel, optimized acquisition techniques for single and multiple kVp coronary angiography and brain perfusion CT scans.

Acknowledgments

This study was supported in part by an appointment to the Research Participation Program at the FDA Center for Devices and Radiological Health administered by the Oak Ridge Institute for Science and Education through an interagency agreement between the United States Department of Energy and the Food and Drug Administration, Office of Women's Health. Computer simulations were performed on the Marquette University Pere High Performance Computing Cluster, which was funded in part by National Science Foundation awards OCI-0923037 and CBET-0521602. The authors would like to thank Lars E. Olson, Ph.D. and David Herzfeld for their support with the high performance cluster.

References

1. National Council on Radiation Protection and Measurements, "Ionizing radiation exposure of the population of the United States," Report No. 160, NCRP, Bethesda, MD, 2009.

2. H. E. Davies, C. G. Wathen, and F. V. Gleeson, "Risks of exposure to radiological imaging and how to minimise them," Br. Med. J. **342**, 589–593 (2011).http://dx.doi.org/10.1136/bmj.d947

3. Committee to Assess Health Risks from Exposure to Low Levels of Ionizing Radiation, Board on Radiation Effects Research, Division of Earth and Life Sciences, National Research Council of The National Academies, Health Risks from Exposure to Low Levels of Ionizing Radiation: BEIR VII Phase 2 (The National Academies Press, Washington, DC, 2006).

4. A. J. Einstein, M. J. Henzlova, and S. Rajagopalan, "Estimating risk of cancer associated with radiation exposure from 64-slice computed tomography coronary angiography," J. Am. Med. Assoc. **298**(3), 317–323 (2007).http://dx.doi.org/10.1001/jama.298.3.317

5. M. S. Pearce, J. A. Salotti, M. P. Little, K. McHugh, C. Lee, K.-P. Kim, N. L. Howe, C. M. Ronckers, P. Rajaraman, A. W. Craft, L. Parker, and A. Berrington de Gonzalez, "Radiation exposure from CT scans in childhood and subsequent risk of leukaemia and brain tumours: A retrospective cohort study," Lancet (in press). Published Online June 7, 2012.http://dx.doi.org/10.1016/S0140-6736(12)60815-0

6. G. Chodick, N. Bekiroglu, M. Hauptmann, B. H. Alexander, D. M. Freedman, M. M. Doody, L. C. Cheung, S. L. Simon, R. M. Weinstock, A. Bouville, and A. J. Sigurdson, "Risk of cataract after exposure to low doses of ionizing radiation: A 20-year prospective cohort study among US radiologic technologists," Am. J. Epidemiol. **168**(6), 620–631 (2008).http://dx.doi.org/10.1093/aje/kwn171

7. E. Nakashima, K. Neriishi, and A. Minamoto, "A reanalysis of atomic-bomb cataract data, 2000-2002: A threshold analysis," Health Phys. **90**(2), 154–160 (2006).http://dx.doi.org/10.1097/01.HP.0000175442.03596.63

8. K. Neriishi, E. Nakashima, A. Minamoto, S. Fujiwara, M. Akahoshi, H. K. Mishima, T. Kitaoka, and R. E. Shore, "Postoperative cataract cases among atomic bomb survivors: Radiation dose response and threshold," Radiat. Res. **168**(4), 404–408 (2007).http://dx.doi.org/10.1667/RR0928.1

9. E. Ainsbury, S. Bouffler, W. Dörr, and J. Graw, "Radiation cataractogenesis: A review of recent studies," Radiat. Res. **172**(1), 1–9 (2009).http://dx.doi.org/10.1667/RR1688.1

10. International Commission on Radiological Protection (ICRP), ICRP ref 4825-3093-1464: Statement on Tissue Reactions, April 2011.

11. Food and Drug Administration (FDA), "Safety Investigation of CT Brain Perfusion Scans" (available URL: http://www.fda.gov/MedicalDevices/Safety/AlertsandNotices/ucm185898.htm). Last accessed May 2011.

12. S. V. Vollmar and W. A. Kalender, "Reduction of dose to the female breast in thoracic CT: A comparison of standard-protocol, bismuth-shielded, partial and tube-current-modulated CT examinations," Eur. Radiol. **18**(8), 1674–1682 (2008).http://dx.doi.org/10.1007/s00330-008-0934-9

13. E. Angel, N. Yaghmai, C. M. Jude, J. J. Demarco, C. H. Cagnon, J. G. Goldin, A. N. Primak, D. M. Stevens, D. D. Cody, C. H. McCollough, and M. F. McNitt-Gray, "Monte Carlo simulations to assess the effects of tube current modulation on breast dose for multidetector CT," Phys. Med. Biol. **54**(3), 497–512 (2009).http://dx.doi.org/10.1088/0031-9155/54/3/003

14. K. H. Chang, W. Lee, D. M. Choo, C. S. Lee, and Y. Kim, "Dose reduction in CT using bismuth shielding: Measurements and Monte Carlo simulations," Radiat. Protect. Dosim. **138**(4), 382–388 (2010).http://dx.doi.org/10.1093/rpd/ncp278

15. C. Coursey, D. P. Frush, T. Yoshizumi, G. Toncheva, G. Nguyen, and S. B. Greenberg, "Pediatric chest MDCT using tube current modulation: Effect on radiation dose with breast shielding," Am. J. Roentgenol. **190**(1), W54–W61 (2008).http://dx.doi.org/10.2214/AJR.07.2017

16. L. M. Hurwitz, T. T. Yoshizumi, P. C. Goodman, R. C. Nelson, G. Toncheva, G. B. Nguyen, C. Lowry, and C. Anderson-Evans, "Radiation dose savings for adult pulmonary embolus 64-MDCT using bismuth breast shields, lower peak kilovoltage, and automatic tube current modulation," Am. J. Roentgenol. **192**(1), 244–253 (2009).http://dx.doi.org/10.2214/AJR.08.1066

17. Imaging Performance Assessment of CT Scanners Group, "ImPACT CT patient dosimetry calculator," (2006) (available URL: http://www.impactscan.org).

18. penEasy software (2010) (available URL: http://inte.upc.edu/downloads).

19. penEasy Imaging software (2010) (available URL: http://code.google.com/p/peneasy-imaging).

20. J. Sempau, A. Badal, and L. Brualla, "A PENELOPE-based system for the automated Monte Carlo simulation of clinacs and voxelized geometries-application to far-from-axis fields," Med. Phys. **38**(11), 5887–5895 (2011).http://dx.doi.org/10.1118/1.3643029

21. F. Salvat, J. Fernández-Varea, and J. Sempau, "PENELOPE-2006: A code system for Monte Carlo simulation of electron and photon transport," in Workshop Proceedings (Nuclear Energy Agency, Organization for Economic Co-operation and Development, Barcelona, Spain, 2006).

22. A. Christ, W. Kainz, E. G. Hahn, K. Honegger, M. Zefferer, E. Neufeld, W. Rascher, R. Janka, W. Bautz, J. Chen, B. Kiefer, P. Schmitt, H.-P. Hollenbach, J. Shen, M. Oberle, D. Szczerba, A. Kam, J. W. Guag, and N. Kuster, "The Virtual Family—Development of surface-based anatomical models of two adults and two children for dosimetric simulations," Phys. Med. Biol. **55**(2), N23–N38 (2010).http://dx.doi.org/10.1088/0031-9155/55/2/N01

23. ICRP, "Adult Reference Computational Phantoms. ICRP Publication 110," Ann. ICRP 39 (2009).

24. H. Woodard and D. White, "The composition of body tissues," Br. J. Radiol. **59**(708), 1209–1219 (1986).http://dx.doi.org/10.1259/0007-1285-59-708-1209

25. M. Cristy and K. F. Eckerman, "Specific absorbed fractions of energy at various ages from internal photon sources," ORNL Report No. TM-8381 (Oak Ridge National Laboratory, Oak Ridge, TN, 1987), Vols. I–VII.

26. Food and Drug Administration (FDA), "Code of Federal Regulations 21 CFR 1020.33(b)(6)" (available URL: http://www.accessdata.fda.gov/scripts/cdrh/cfdocs/cfcfr/CFRSearch.cfm?FR=1020.33). Last accessed April 2011.

27. A. J. Einstein, C. D. Elliston, A. E. Arai, M. Y. Chen, R. Mather, G. D. N. Pearson, R. L. DeLaPaz, E. Nickoloff, A. Dutta, and D. J. Brenner, "Radiation dose from single-heartbeat coronary CT angiography performed with a 320-detector row volume scanner," Radiology **254**(3), 698–706 (2010).http://dx.doi.org/10.1148/radiol.09090779

28. E. J. Salomon, J. Barfett, P. W. A. Willems, S. Geibprasert, S. Bacigaluppi, and T. Krings, "Dynamic CT angiography and CT perfusion employing a 320-detector row CT," Clin. Neuroradiol. **19**(3), 187–196 (2009).http://dx.doi.org/10.1007/s00062-009-9019-7

29. S. Abboud, R. J. Jennings, S. H. Stern, M. Mahesh, and I. Kyprianou, "A method to characterize the shaped filtration associated with angle-

dependent spectra of clinical computed tomography (CT) systems," Med. Phys. (submitted).

30. S. E. McKenney, A. Nosratieh, D. Gelskey, K. Yang, S.-y. Huang, L. Chen, and J. M. Boone, "Experimental validation of a method characterizing bow tie filters in CT scanners using a real-time dose probe," Med. Phys. **38**(3), 1406–1415 (2011).http://dx.doi.org/10.1118/1.3551990

31. C. Lee, C. Lee, A. P. Shah, and W. E. Bolch, "An assessment of bone marrow and bone endosteum dosimetry methods for photon sources," Phys. Med. Biol. **51**, 5391–5407 (2006).http://dx.doi.org/10.1088/0031-9155/51/21/001

32. M. Rosenstein, Organ Doses in Diagnostic Radiology (HEW Publication, FDA 76-8030, Food and Drug Administration, Rockville, MD, 1976).

33. A. C. Turner, M. Zankl, J. J. DeMarco, C. H. Cagnon, D. Zhang, E. Angel, D. D. Cody, D. M. Stevens, C. H. McCollough, and M. F. McNitt-Gray, "The feasibility of a scanner-independent technique to estimate organ dose from MDCT scans: Using CTDI to account for differences between scanners," Med. Phys. **37**(4), 1816–1825 (2010).http://dx.doi.org/10.1118/1.3368596

34. J. H. Hubbell and S. M. Seltzer, "Tables of x-ray mass attenuation coefficients and mass-energy absorption coefficients" (1996) (available URL: http://physics.nist.gov/PhysRefData/XrayMassCoef/tab3.html).

35. J. Boone, "The trouble with CTDI100," Med. Phys. **34**(4), 1364–1371 (2007).http://dx.doi.org/10.1118/1.2713240

36. International Electrotechnical Commission, IEC Publication 60601: Medical Electrical Equipment, Part 2-44: Particular Requirements for the Safety of X-ray Equipment for Computed Tomography (International Electrotechnical Commission, Geneva, Switzerland, 2002).

37. K. Cranley, B. Gilmore, G. W. A. Fogarty, and L. Desponds, "Catalogue of diagnostic x-ray spectra and other data," Report No. 78 (The Institute of Physics and Engineering in Medicine (IPEM), 1997).

38. A. C. Turner, D. Zhang, M. Khatonabadi, M. Zankl, J. J. DeMarco, C. H. Cagnon, D. D. Cody, D. M. Stevens, C. H. McCollough, and M. F. McNitt-Gray, "The feasibility of patient size-corrected, scanner-

independent organ dose estimates for abdominal CT exams," Med. Phys. **38**(2), 820–829 (2011).http://dx.doi.org/10.1118/1.3533897

39. F. Rupcich, I. Kyprianou, A. Badal, and T. Gilat-Schmidt, "Energy deposition in the breast during CT scanning: Quantification and implications for dose reduction," in Proceedings of SPIE—Medical Imaging 2011: Physics of Medical Imaging, edited by N. J. Pelc, E. Samei, and R. M. Nishikawa (SPIE, Lake Buena Vista, FL, 2011), Vol. 7961.

40. M. Gies, W. A. Kalender, H. Wolf, C. Suess, and M. T. Madsen, "Dose reduction in CT by anatomically adapted tube current modulation. I. Simulation studies," Med. Phys. **26**(11), 2235–2257 (1999).http://dx.doi.org/10.1118/1.598779

41. S. J. Glick, S. Thacker, X. Gong, and B. Liu, "Evaluating the impact of x-ray spectral shape on image quality in flat-panel CT breast imaging," Med. Phys. **34**(1), 5–24 (2007).http://dx.doi.org/10.1118/1.2388574

42. R. L. McKinley, M. P. Tornai, E. Samei, and M. L. Bradshaw, "Simulation study of a quasi-monochromatic beam for x-ray computed mammotomography," Med. Phys. **31**(4), 800–813 (2004).http://dx.doi.org/10.1118/1.1668371

43. D. Jones and P. Shrimpton, Survey of CT Practice in the UK Part 3: Normalised Organ Doses Calculated Using the Monte Carlo Techniques, NRPB-R250 (National Radiological Protection Board, Oxon, United Kingdom, 1991).

44. M. Zankl, W. Panzer, and G. Drexler, The Calculation of Dose from External Photon Exposures Using Reference Human Phantoms and Monte Carlo Methods. Part VI: Organ Doses from Computed Tomographic Examinations, GSF-Bericht 30/91 (GSFÑ Forschungszentrum fur Umwelt und Gesundtheit, Institut fur Strahlenschutz, Neuherberg, Germany, 1991).

45. J. J. DeMarco, C. H. Cagnon, D. D. Cody, D. M. Stevens, C. C. McCollough, M. Zankl, E. Angel, and M. F. McNitt-Gray, "Estimating radiation doses from multidetector CT using Monte Carlo simulations: Effects of different size voxelized patient models on magnitudes of organ and effective dose," Phys. Med. Biol. **57**, 2583–2597 (2007).http://dx.doi.org/10.1088/0031-9155/52/9/017

46. J. M. Boone, E. M. Geraghty, J. A. Seibert, and S. L. Wootton-Gorges, "Dose reduction in pediatric CT: A rational approach," Radiology **228**(2), 352–360 (2003).http://dx.doi.org/10.1148/radiol.2282020471

47. T. R. C. Johnson, B. Krauß, M. Sedlmair, M. Grasruck, H. Bruder, D. Morhard, C. Fink, S. Weckbach, M. Lenhard, B. Schmidt, T. Flohr, M. F. Reiser, and C. R. Becker, "Material differentiation by dual energy CT: Initial experience," Eur. Radiol. **17**(6), 1510–1517 (2006).http://dx.doi.org/10.1007/s00330-006-0517-6

48. M. M. Goodsitt, E. G. Christodoulou, and S. C. Larson, "Accuracies of the synthesized monochromatic CT numbers and effective atomic numbers obtained with a rapid kVp switching dual energy CT scanner," Med. Phys. **38**(4), 2222–2232 (2011).http://dx.doi.org/10.1118/1.3567509

49. A. N. Primak, J. C. Ramirez Giraldo, X. Liu, L. Yu, and C. H. McCollough, "Improved dual-energy material discrimination for dual-source CT by means of additional spectral filtration," Med. Phys. **36**(4), 1359–1369 (2009).http://dx.doi.org/10.1118/1.3083567

50. A. N. Primak, J. C. R. Giraldo, C. D. Eusemann, B. Schmidt, B. Kantor, J. G. Fletcher, and C. H. McCollough, "Dual-source dual-energy CT with additional tin filtration: Dose and image quality evaluation in phantoms and in vivo," Am. J. Roentgenol. **195**(5), 1164–1174 (2010).http://dx.doi.org/10.2214/AJR.09.3956

51. http://www.eng.mu.edu/medicalimaging/dose_database.

52. See supplementary material at http://dx.doi.org/10.1118/1.4739243 for the tables of normalized dose deposition. [Supplementary Material]

About the Authors

Franco Rupcich - franco.rupcich@mu.edu
Department of Biomedical Engineering, Marquette University, Milwaukee, Wisconsin 53233
Andreu Badal - Andreu.Badal-Soler@fda.hhs.gov
and Iacovos Kyprianou - Iacovos.Kyprianou@fda.hhs.gov
Division of Imaging and Applied Mathematics (OSEL/CDRH), US Food and Drug Administration, Silver Spring, Maryland 20905
Taly Gilat Schmidt - taly.gilat-schmidt@mu.edu

Department of Biomedical Engineering, Marquette University, Milwaukee, Wisconsin 53233

Medical Physics, Vol. 39, No. 9 (September 2012): pg. 5336-5346. DOI.